Grain boundary characteristics of oxypnictide NdFeAs(O,F) superconductors

Kazumasa Iida[1,2], Taito Omura[2], Takuya Matsumoto[1], Takafumi Hatano[1,2], Hiroshi Ikuta[1,2]

[1]Department of Materials Physics, Nagoya University, Furo-cho, Chikusa-ku, Nagoya 464-8603, Japan

[2]Department of Crystalline Materials Science, Nagoya University, Furo-cho, Chikusa-ku, Nagoya 464-8603, Japan

E-mail: iida@mp.pse.nagoya-u.ac.jp

Abstract. We have systematically investigated the grain boundary angle (θ_{GB}) dependence of transport properties for NdFeAs(O,F) fabricated on [001]-tilt symmetric MgO bicrystal substrates. In our previous study, NdFeAs(O,F) bicrystal films showed a weak-link behaviour even at a θ_{GB} of 6°. However, this was caused by an extrinsic effect originating from the damage to both NdFeAs(O,F) and MgO substrate by excess F-diffusion along the grain boundary. To investigate the intrinsic nature of grain boundaries, we minimized the damage to NdFeAs(O,F) and MgO by reducing the deposition temperature of NdOF over-layer needed for F-doping. The resultant NdFeAs(O,F) bicrystal films have a critical angle of 8.5°, above which J_c starts to decrease exponentially. This critical angle is almost the same as those of other Fe-based superconductors.

1. Introduction

The discovery of iron-based superconductors (FBS) triggered a huge excitement for the community of fundamental and applied superconductivity research. Since then many physical quantities of FBS have been revealed, e.g. the coherence length is short, which results from the small Fermi velocity and low carrier density [1]. The in-plane coherence length $\xi_{ab}(0)$ at zero kelvin obtained from upper critical field measurements is 2∼4 nm for FBS [e.g. the respective $\xi_{ab}(0)$ for Fe(Se,Te), $BaFe_2(As_{0.7}As_{0.3})_2$, $(Ba,K)Fe_2As_2$, $NdFeAsO_{0.8}F_{0.2}$, and SmFeAs(O,F) were 1.5 nm [2], 2.1 nm [3], 1.6 nm [4], 3.9 nm [5], and 1.4 nm [6]], which is similar to that for the cuprates. This short coherence length arouses concern that the superconductivity of FBS at grain boundaries may be depressed by crystalline disorder. However, the symmetry of the superconducting order parameter of FBS is reported to be an extended *s*-wave [7, 8, 9], which differs from the *d*-wave of the cuprates [10]. Hence, the critical current density (J_c) of FBS across the GB is expected to be not as severely reduced as cuprates. In fact, the critical angle (θ_c), above which J_c starts to decrease exponentially, is around 9° for Co-doped $BaFe_2As_2$ (Ba-122) [11] and Fe(Se,Te) [12, 13], much larger than $YBa_2Cu_3O_7$ (θ_c=3°∼5°) [14]. Additionally, the grain boundaries for Co- and P-doped Ba-122 [11, 15], and Fe(Se,Te) [12, 13] are of metallic nature. Both of these features are favourable for high-field conductor applications.

Among the various FBS *Ln*FeAs(O,F) (*Ln*: lanthanoide) has the highest superconducting transition temperature (T_c), which yields a large margin between T_c and the temperature where a cryocooler can reach. Hence, SmFeAs(O,F) wires [16] and NdFeAs(O,F) tapes [17] have been demonstrated as proof-of-principle studies for conductor applications. However, a large J_c gap between those conductors and the counterpart of single crystals or epitaxial thin films was recognised [18]. To understand the reason for such performance gap, GB characteristics of *Ln*FeAs(O,F) should be clarified.

Previously, we have investigated the grain boundary angle (θ_{GB}) dependence of inter-grain J_c (J_c^{GB}) for NdFeAs(O,F) grown on [001]-tilt symmetric MgO bicrystal substrates [19]. As a result, J_c^{GB} for θ_{GB}=6° was reduced by nearly 30% compared to the intra-grain J_c (J_c^{Grain}). Microstructural investigation by transmission electron microscope (TEM) revealed that fluorine preferentially diffused through GB and thereby eroded NdFeAs(O,F) and the substrate. Hence, suppressing the excess diffusion of F is the key to exploring the intrinsic grain boundary properties. In the aforementioned study, F-doping has been conducted by a NdOF over-layer method [20], where parent NdFeAsO was deposited at 800°C, followed by the deposition of NdOF at the same temperature. Here, a growth temperature of 800°C was necessary for achieving high crystallinity of NdFeAsO [21]. On the other hand, the deposition temperature (T_{dep}) of NdOF would not affect the crystalline quality of NdFeAs(O,F). Hence, it is possible to suppress the excess F diffusion by lowering T_{dep} of NdOF. However, the lack of F leads to low-T_c or even non-superconducting NdFeAs(O,F) films. Therefore, NdFeAs(O,F)

bicrystal films should be fabricated by employing a T_{dep} of NdOF as low as possible without compromising the superconducting properties.

In this paper, we firstly determine the lowest T_{dep} for the NdOF over-layer that results into a NdFeAs(O,F) film with a sufficiently high T_c by mapping the diagram of T_c versus T_{dep}. Then NdFeAs(O,F) bicrystal films are fabricated by employing the thus determined T_{dep} for NdOF, followed by structural characterisations as well as transport measurements.

2. Experiment

NdFeAs(O,F) thin films were grown on MgO(001) single crystalline substrates by molecular beam epitaxy (MBE) using solid sources of Fe, Fe_2O_3, As, NdF_3 and Ga. Here, Ga was used as a F-getter to adjust the amount of fluorine [22]. A two-step process was employed to grow superconducting NdFeAs(O,F) thin films: parent NdFeAsO films of 40 nm thickness were grown at 800°C, followed by the deposition of 12 nm thick NdOF in the temperature range 600°C $\leq T_{dep} \leq$ 800°C. For identifying the lowest deposition temperature of NdOF, T_c of the resultant NdFeAs(O,F) films was plotted as a function of T_{dep} (see fig. 2). After determination of the lowest T_{dep} of NdOF, NdFeAs(O,F) thin films were fabricated on [001]-tilt symmetric MgO bicrystal substrates (θ_{GB}=6°, 9°, 12°, 24°) by the two-step process, whereas the respective thicknesses of NdFeAsO and NdOF were 160 nm and 50 nm to maintain the thickness ratio of NdOF to NdFeAsO as around 0.3.

Phase purity and *c*-axis texture were examined by x-ray diffraction (XRD) in Bragg-Brentano geometry using Cu-Kα radiation. In-plane orientation of NdFeAs(O,F) was investigated by the ϕ-scan of the 102 peak. After structural characterisation by XRD, the NdOF over-layer was removed by Ar-ion milling. Microstructural analyses on the NdFeAs(O,F) bicrystal film with θ_{GB}=6° were performed by TEM. From the TEM image of cross-sectional view away from the GB region, the thickness of NdFeAs(O,F) was found to be around 130 nm after Ar-ion milling.

For transport measurements of both inter- and intra-grain J_c, two micro-bridges were fabricated on the same film. The thin films were patterned by a photolithography method and then etched by Ar-ion milling to form micro-bridges. The bridges were 20-40 µm-wide and 1 mm-long across the grain boundary and 0.25 mm-long away from the grain boundary. Transport properties using the resultant bridges were measured by a four-probe method. The onset T_c was determined as the intersection between the fit to the normal state resistivity and the steepest slope of resistivity. An electric field criterion of E=1 µV/cm was applied for evaluating intra-grain J_c (J_c^{Grain}) and inter-grain J_c (J_c^{GB}) for θ_{GB}=6° and 9°. J_c^{GB} for θ_{GB}=12° was defined as the intersection between $E = 0$ and a linear fit to the non-ohmic linear differential (NOLD) region (i.e. the region where E increased linearly with the current density J).

3. Results and discussion

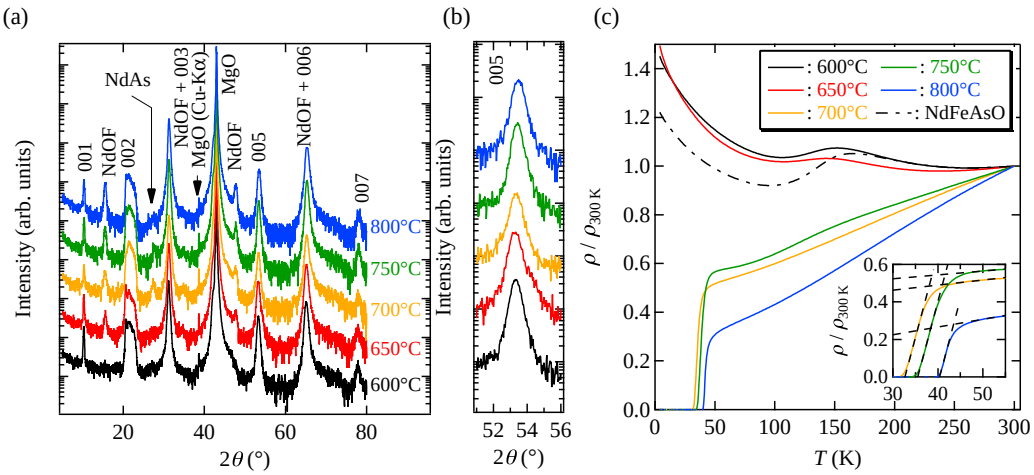

Figure 1. (a) The $\theta/2\theta$-scans (Cu-Kα) of the NdFeAs(O,F) thin films for various deposition temperatures of the NdOF over-layer. (b) Enlarged view of the 005 reflection. (c) The normalised resistivity curves of the NdFeAs(O,F) thin films for various deposition temperatures of the NdOF over-layer. For comparison, the data of the parent NdFeAsO film is also plotted. The data were normalised to the value of 300 K. Inset shows the enlarged view of the superconducting transition. The dashed lines are fits to the normalised traces in the region of the transition and the normal states.

Figure 1(a) shows the XRD patterns of the NdFeAs(O,F) thin films for various deposition temperatures of the NdOF over-layer. All NdFeAs(O,F) films were grown *c*-axis oriented. The diffraction peak of NdAs, which is a by-product of chemical reaction between NdOF and NdFeAsO, appeared above $T_{\rm dep}$=700°C. This is a natural consequence that higher deposition temperatures stimulate the chemical reaction. Another feature is a shift of the 00*l* reflections to higher angles with increasing $T_{\rm dep}$, indicative of shortening the *c*-axis length [fig. 1(b)]. It was reported that the *c*-axis lattice parameter of $LaFeAsO_{1-x}F_x$ [23] and $CeFeAsO_{1-x}F_x$ [24] monotonously decreased with increasing F content. Hence, the observed change indicates that F diffuses into NdFeAsO and the amount of F in NdFeAs(O,F) increased with increasing the deposition temperature of the NdOF over-layer.

The temperature dependence of the normalised resistivity ($\rho/\rho_{300\,\rm K}$) varies with $T_{\rm dep}$ [fig. 1(c)]. Below $T_{\rm dep}$=650°C the normalised resistivity curves of the films were almost similar to those of the parent NdFeAsO. The upturn of $\rho/\rho_{300\,\rm K}$ at around 150 K corresponds to the structural transition from a high temperature tetragonal phase to a low temperature orthorhombic one. An onset $T_{\rm c}$ of 38 K was recorded for the film with $T_{\rm dep}$=700°C. Further increase of the $T_{\rm dep}$ leads to an improvement of $T_{\rm c}$.

Figure 2 summarises the *c*-axis lattice parameter and $T_{\rm c}$ for the NdFeAs(O,F) films as a function of deposition temperature of NdOF. The *c*-axis lattice parameter decreased almost linearly with increasing $T_{\rm dep}$. Superconductivity can be induced by

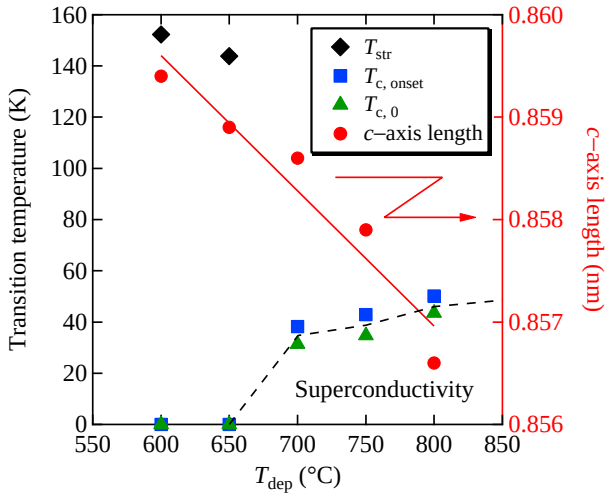

Figure 2. The transition temperatures and the c-axis lattice parameters for the NdFeAs(O,F) films as a function of the deposition temperature (T_{dep}) of NdOF. The black diamond, blue square, green triangle, and red circle represent the structural transition temperature (T_{str}), the onset superconducting transition temperature ($T_{c,onset}$), the zero resistance temperature ($T_{c,0}$), and the c-axis length, respectively. Note that the films with T_{dep}=600°C and 650°C did not show superconductivity. Red and dashed lines are guides for the eye.

the deposition of NdOF at $T_{dep} > 650$°C. From these results, the lowest T_{dep} with keeping superconductivity is determined to be 700°C. In the following results, the NdOF over-layer was deposited at 700°C.

Structural characterisation of the NdFeAs(O,F) films grown on [001]-tilt symmetric MgO bicrystal substrates is summarised in fig. 3. The $\theta/2\theta$-scans showed that the NdFeAs(O,F) films were c-axis oriented. The azimuthal ϕ-scan of the off-axis 102 reflection of NdFeAs(O,F) showed clearly eight peaks from two adjacent NdFeAs(O,F) grains separated by θ_{GB} [fig. 3(b)]. Hence, the NdFeAs(O,F) films were grown epitaxially on [001]-tilt symmetric MgO bicrystal substrates.

In fig. 4(a) the resistivity curves for the inter-grain bridges (bridge width w=30 μm) with various misorientation angles are shown. For comparison the data of the intra-grain bridge (θ_{GB}=0°) fabricated from the NdFeAs(O,F) film with θ_{GB}=6° are also plotted. As can be seen, the superconducting transition temperature did not systematically change with the grain boundary angle, which differs from our previous study (i.e. T_c decreased with increasing θ_{GB}) [19]. The inter-grain bridges with θ_{GB}=6° and 12° had an onset T_c ($T_{c,onset}$) of 45 K, which is almost the same as for the intra-grain bridges. For $\theta_{GB} \geq 9°$ a wide transition width of 5 K was observed. As shown in Supplementary fig. S1, almost no difference in T_c as well as the superconducting transition width were found with changing the bridge width.

A finite resistivity was observed for the inter-grain bridge with θ_{GB}=24° below T_c, whereas the other bridges showed a resistivity well below the instrumental limitation. Hence, the grain boundary region for θ_{GB}=24° was destroyed by F even at T_{dep}=700°C,

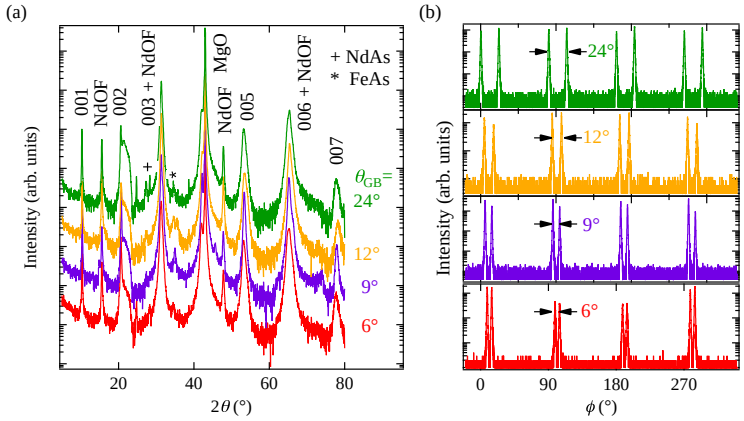

Figure 3. Summary of the structural characterisation for the NdFeAs(O,F) thin films fabricated on [001]-tilt symmetric MgO bicrystal substrates having various θ_{GB}. (a) The $\theta/2\theta$-scans and (b) the azimuthal ϕ-scans of the off-axis 102 reflection of NdFeAs(O,F).

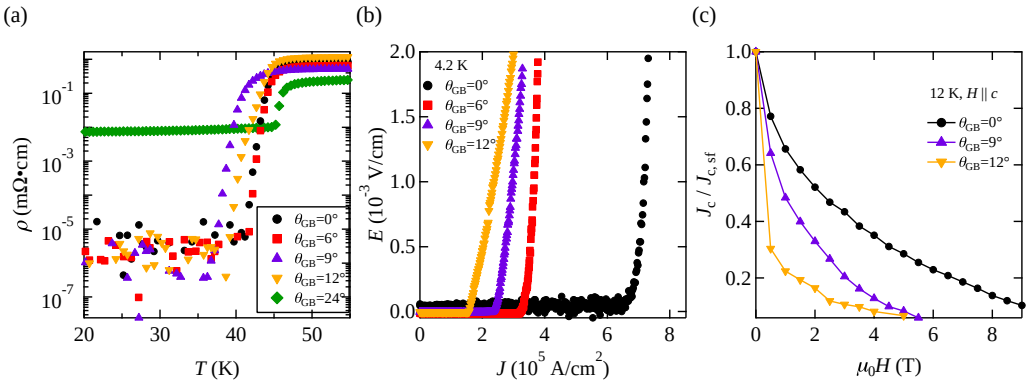

Figure 4. (a) Semi-logarithmic plot of the resistivity curves for the inter-grain bridges having various θ_{GB} and the intra-grain bridge (θ_{GB}=0°). The intra-grain bridge was fabricated from the NdFeAs(O,F) film with θ_{GB}=6°. The measurements were conducted using 30 µm-wide bridges. (b) $E-J$ curves of the inter-grain bridges of 30 µm-wide for various θ_{GB} and the intra-grain bridge (θ_{GB}=0°) measured at 4.2 K without magnetic field. The intra-grain bridge was fabricated from the NdFeAs(O,F) film with θ_{GB}=12°. (c) Comparative field dependence of J_c normalised to the self-field J_c ($J_{c,sf}$) measured at 12 K for $H \| c$. The bridges are the same as those presented in (b).

and accordingly, J_c across the GB is zero.

Figure 4(b) compares the $E-J$ curves for the inter-grain bridges with various θ_{GB} measured at 4.2 K without a magnetic field. The curve for the intra-grain bridge (θ_{GB}=0°) is also included, which exhibited a power-law behaviour described by $E \sim J^n$, representing flux creep effects. The same behaviour was also seen for the inter-grain bridges with θ_{GB}=6° and 9°, which indicates that the two adjacent grains were strongly coupled. On the other hand, the inter-grain curve for θ_{GB}=12° showed a non-Ohmic linear differential (NOLD) behaviour (i.e. E is linearly changing

with J) originating from viscous flux flow along the grain boundaries [25], indicative of J_c limitation by grain boundaries [26]. The resistance area product for θ_{GB}=12° was estimated to be $8.5\times10^{-10}\,\Omega\mathrm{cm}^2$, which is of the same order of magnitude for Co-doped Ba-122 with θ_{GB}=45° ($5\times10^{-10}\,\Omega\mathrm{cm}^2$)[11], P-doped Ba-122 with θ_{GB}=24° ($1.3\times10^{-10}\,\Omega\mathrm{cm}^2$)[15], and Fe(Se,Te) with θ_{GB}=24° ($7\times10^{-10}\,\Omega\mathrm{cm}^2$)[12]. Hence, the grain boundary of NdFeAs(O,F) is of metallic nature, which is similar to other FBS.

The field dependence of J_c normalised to the self-field J_c ($J_{c,sf}$) plotted in fig. 4(c) also shows a typical behaviour of GB transport observed for FBS. For the bridge with θ_{GB}=12°, inter-grain J_c was decreased by 70% even at a small applied magnetic field of 0.5 T, whereas the corresponding reduction for θ_{GB}=0° (i.e. intra-grain) and θ_{GB}=9° were 23% and 36%, respectively. Such a sharp drop of inter-grain J_c for large θ_{GB} by small magnetic fields is due to the weak coupling nature between adjacent grains.

To further characterise the coupling between the grains with θ_{GB}=6°, microstructural observation by TEM was conducted [fig. 5(a)]. For comparison, the microstructures away from the GB region are also shown in fig. 5(b). The elemental mappings revealed a uniform distribution of all elements except for O and F [fig. 5(b)]. The observed high concentration of O and F at the surface region may be caused by heating due to Ar-ion milling to remove the NdOF over-layer. Uniform distribution of Nd, Fe, As, O and F within NdFeAs(O,F) was also observed in a different bridge (see Supplementary fig. S2). In stark contrast, the elemental distribution of the top region of NdFeAs(O,F) around the GB was strongly inhomogeneous due to the damage to NdFeAs(O,F) by F even though the deposition temperature of the NdOF over-layer was lowered [fig. 5(a)]. This is very similar to what was observed in our previous investigation[19]. However, the bottom region (about half of the thickness from the substrate) was quite uniform and free from damage by F. Hence, the grains are still coupled strongly in this region.

The temperature dependence of self-field J_c for various misorientation angles are summarised in figs. 6(a)–(c). The intra-grain J_c (J_c^{Grain}) of each film is also shown for comparison. Here, the measurements were conducted using 30 µm-wide bridges. The results obtained from various bridges are summarised in Supplementary fig. S3. The self-field J_c of the intra-grain at low temperatures is in the order of $10^5\,\mathrm{A/cm}^2$ for all three samples, which is one order of magnitude lower than our NdFeAs(O,F) films grown by employing T_{dep}=800°C [27]. By comparing the J_c^{Grain} at the same reduced temperatures ($t = T/T_c$), J_c^{Grain} of an ordinal NdFeAs(O,F) film prepared with T_{dep}=700°C is smaller than that of a film with T_{dep}=800°C [fig. 6(d)]. This is due to low carrier concentration. Hall effect measurements on our NdFeAs(O,F) films grown on single crystalline MgO revealed that the carrier concentration decreased from $1.98\times10^{21}\,/\mathrm{cm}^3$ for T_{dep}=800°C to $1.34\times10^{21}\,/\mathrm{cm}^3$ for T_{dep}=750°C at 50 K [28], although a precise evaluation of the carrier concentration is not easy due to the multi-band nature of the current superconductor. The carrier concentration of NdFeAs(O,F) for T_{dep}=700°C is expected to be even smaller than that for T_{dep}=750°C, which probably explains the smaller J_c.

The distinct feature of the above results is that the respective inter-grain critical current densities (J_c^{GB}) for θ_{GB}=6° and 9° are almost comparable to their intra-grain J_c

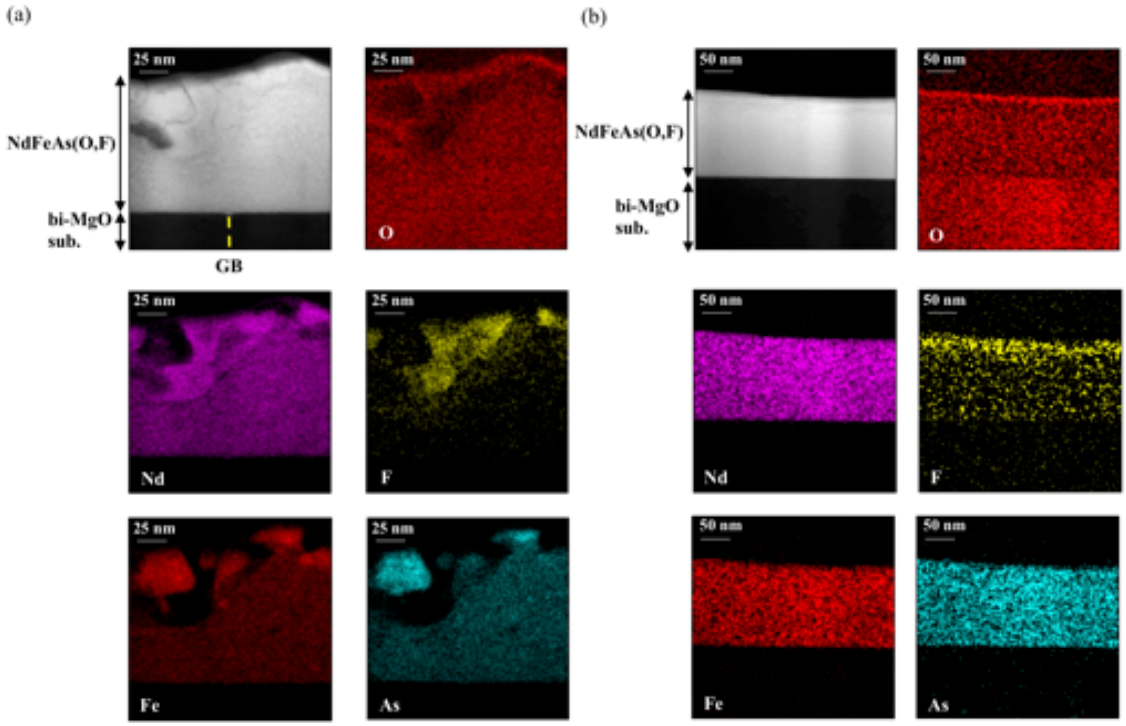

Figure 5. (a) TEM micrograph of a cross section of the GB region having θ_{GB}=6° and the elemental mappings at the same area. The location of the GB is indicated by a dashed yellow line in the micrograph. (b) The microstructures away from the GB region. The thickness of NdFeAs(O,F) was around 130 nm.

(J_c^{Grain}) at all temperatures [figs. 6(a), (b)], indicative of the absence of weak-links for both bicrystal films. For θ_{GB}=12° J_c^{GB} below 32 K was certainly lower than J_c^{Grain}. In Cu-Ag alloys it has been observed that the GBs are completely wetted by Ag when the misorientation angle is large [29]. It might be possible that F-rich phase had covered GBs and caused the transition from strong-link to weak-link behaviour. Nevertheless,

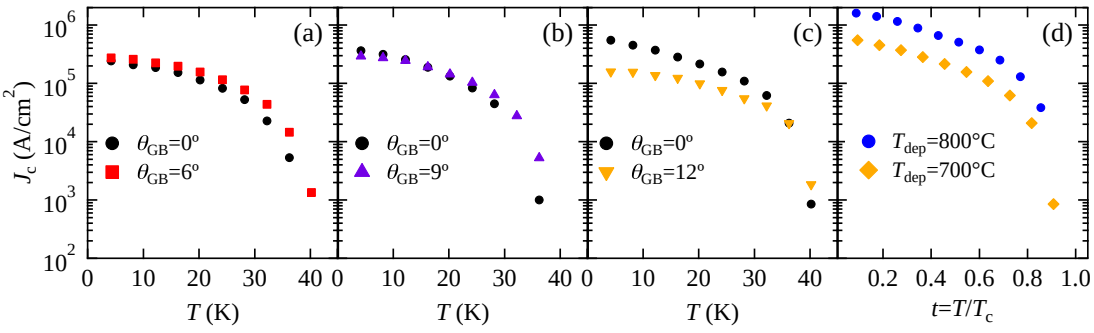

Figure 6. (a)–(c) Temperature dependence of the self-field J_c for the intra- and inter-grain bridges (bridge width w=30 µm) having various θ_{GB}. (d) Self-field J_c^{Grain} as a function of reduced temperature for NdFeAs(O,F) films grown by employing T_{dep}=700°C and 800°C.

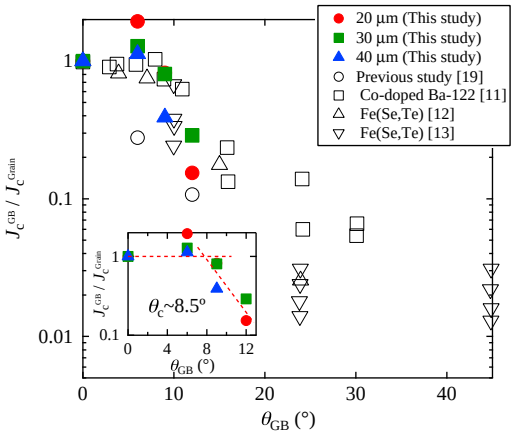

Figure 7. The ratio of inter- to intra-grain J_c (J_c^{GB}/J_c^{Grain}) at 4.2 K for NdFeAs(O,F) bicrystal films as a function of θ_{GB}. The data of Co-doped Ba-122 at 4 K [11], Fe(Se,Te) at 4.2 K [12, 13], and our previous study on NdFeAs(O,F) at 4.2 K [19] are also plotted for comparison. Inset shows an enlarged view in the vicinity of the critical angle (θ_c).

J_c^{GB} at 4.2 K decreased by only 28% compared to J_c^{Grain} in stark contrast to our previous study [19]. Note that the effective cross-sectional area in the vicinity of the GB with θ_{GB}=6° was smaller than the intra-grain bridge as a consequence of the damage caused by F diffusion [see fig. 5(a)]. This is probably the reason why the plotted J_c^{GB} values are higher than J_c^{Grain} in fig. 6(a), since J_c was calculated by assuming that both the inter- and intra-grain bridges have the identical thickness.

Figure 7 shows the θ_{GB} dependence of the ratio of inter- to intra-grain J_c (J_c^{GB}/J_c^{Grain}) for the NdFeAs(O,F) bicrystal films at 4.2 K. For comparison the data of Co-doped Ba-122 at 4 K [11], Fe(Se,Te) at 4.2 K [12, 13], and our previous work on NdFeAs(O,F) at 4.2 K [19] are also plotted. The present work on NdFeAs(O,F) bicrystal films showed that J_c^{GB}/J_c^{Grain} was unity up to 8.5° (i.e. $\theta_c = 8.5°$), followed by a decrease with θ_{GB}. On the other hand, θ_c was less than 6° in our previous investigation. These results indicate that the grain boundary properties were improved by lowering T_{dep} of NdOF. It is interesting that all FBS have a similar critical angle of around 9°, suggesting that the symmetry of the superconducting order parameter for NdFeAs(O,F) may be the same as Co-doped Ba-122 and Fe(Se,Te).

Although θ_c=8.5° was determined for NdFeAs(O,F), it is still ambiguous how the inter-grain J_c decreases with θ_{GB} beyond 12°. Additionally, it is not ruled out completely that the damage to the GB region by F had influenced the obtained results. To answer these issues and explore further the intrinsic GB characteristics, studying F-free oxypnictides, e.g. $Ln(Fe_{1-x}Co_x)AsO$ [30, 31], would be interesting. Albeit the highest T_c is around 25 K for $Nd(Fe_{1-x}Co_x)AsO$ [31], there would be no damage to the GB region by F. The misorientation angle dependence of J_c^{GB} for $Nd(Fe_{1-x}Co_x)AsO$ bicrystal films would be the direction of our future studies.

4. Summary

NdFeAs(O,F) epitaxial thin films were fabricated by MBE using a two-step process, where the deposition temperature (T_{dep}) of NdOF was varied in the temperature range 600°C $\leq T_{dep} \leq$ 800°C. The *c*-axis lattice parameter and T_c of NdFeAs(O,F) changed systematically with T_{dep} of NdOF, and the F content in NdFeAs(O,F) increased with increasing T_{dep}. The lowest T_{dep} of NdOF without compromising T_c was determined as 700°C. By using T_{dep}=700°C epitaxial NdFeAs(O,F) thin films were grown on [001]-tilt symmetric MgO bicrystal substrates with θ_{GB}=6°, 9°, 12° and 24°. Even for this reduced T_{dep}, however, the inter-grain bridge with θ_{GB}=24° showed a finite resistance and hence J_c was zero due to the erosion of NdFeAs(O,F) by F. Additionally, J_c of the inter-grain bridges with $\theta_{GB} \leq \theta_c$ and the intra-grain bridge were around 10^5 A/cm^2 at low temperatures, which is almost one order of magnitude lower than NdFeAs(O,F) with T_{dep}=800°C due probably to low carrier concentration. Nevertheless, the GB properties of the inter-grain bridges with lower θ_{GB} were improved, resulting in a critical angle of θ_c=8.5°. This critical angle is identical to Co-doped Ba-122 and Fe(Se,Te).

Acknowledgments

This work was supported by the JSPS Grant-in-Aid for Scientific Research (B) Grant Number 16H04646 as well as JST CREST Grant Number JPMJCR18J4.

References

[1] Putti M, Pallecchi I, Bellingeri E, Cimberle M R, Tropeano M, Ferdeghini C, Palenzona A, Tarantini C, Yamamoto A, Jiang J, Jaroszynski J, Kametani F, Abraimov D, Polyanskii A, Weiss J D, Hellstrom E E, Gurevich A, Larbalestier D C, Jin R, Sales B C, Sefat A S, McGuire M A, Mandrus D, Cheng P, Jia Y, Wen H H, Lee S and Eom C B, 2010 *Supercond. Sci. Technol.* **23** 034003

[2] Klein T, Braithwaite D, Demuer A, Knafo W, Lapertot G, Marcenat C, Rodière P, Sheikin I, Strobel P, Sulpice A and Toulemonde P, 2010 *Phys. Rev. B* **82** 184506

[3] Chaparro C, Fang L, Rydh A, Crabtree G W, Stantev V, Kwok W K and Welp U, 2012 *Phys. Rev. B* **85** 184525

[4] Kacmarcik J, Marcenat C, Klein T, Pribulova Z, van der Beek C J, Konczykowski M, Budko S L, Tillman M, Ni N and Canfield P C, 2009 *Phys. Rev. B* **80** 014515

[5] Adamski A, Krellner C and Abdel-Hafiez M, 2017 *Phys. Rev. B* **96** 100503

[6] Welp U, Chaparro C, Koshelev A E, Kwok W K, Rydh A, Zhigadlo N D, Karpinski J and Weyeneth S, 2011 *Phys. Rev. B* **83** 100513

[7] Mazin I I, Singh D J, Johannes M D and Du M H, 2008 *Phys. Rev. Lett.* **101** 057003

[8] Kuroki K, Onari S, Arita R, Usui H, Tanaka Y, Kontani H and Aoki H 2009 *Phys. Rev. Lett.* **101** 087004

[9] Hanaguri T, Niitaka S, Kuroki K and Takagi H 2010 *Science* **328** 474

[10] Tsuei C C and Kirtley J R 2000 *Rev. Mod. Phys.* **72** 969

[11] Katase T, Ishimaru Y, Tsukamoto A, Hiramatsu H, Kamiya T, Tanabe K and Hosono H 2011 *Nat. Commun.* **2** 409

[12] Si W, Zhang C, Shi X, Ozaki T, Jaroszynsski J and Li Q 2015 *Appl. Phys. Lett.* **106** 032602

[13] Sarnelli E, Nappi C, Camerlingo C, Enrico E, Bellingeri E, Kawale S, Braccini V, Leveratto A and Ferdeghini C 2017 *IEEE. Trans. Appl. Supercond.* **27** 7400104
[14] Hilgenkamp H and Mannhart J 2002 *Rev. Mod. Phys.* **74** 485
[15] Sakagami A, Kawaguchi T, Tabuchi M, Ujihara T, Takeda Y and Ikuta H 2013 *Physica C* **494** 181
[16] Zhang Q, Zhang X, Yao C, Huang H, Wang D, Dong C, Ma Y, Ogino H and Awaji S 2017 *Supercond. Sci. Technol.* **30** 065004
[17] Iida K, Kurth F, Chihara M, Sumiya N, Grinenko V, Ichinose A, Tsukada I, Hänisch J, Matias V, Hatano T, Holzapfel B and Ikuta H 2014 *Appl. Phys. Lett.* **105** 172602
[18] Iida K, Hänisch J and Tarantini C 2018 *Appl. Phys. Rev.* **5** 031304
[19] Omura T, Matsumoto T, Hatano T, Iida K and Ikuta H 2018 *J. Phys.: Conf. Ser.* **1054** 012024
[20] Kawaguchi T, Uemura H, Ohno T, Tabuchi M, Ujihara T, Takenaka K, Takeda Y and Ikuta H 2010 *Appl. Phys. Lett.* **97** 042509
[21] Chihara M, Sumiya N, Arai K, Ichinose A, Tsukada I, Hatano T, Iida K and Ikuta H 2015 *Physica C* **518** 69
[22] Kawaguchi T, Uemura H, Ohno T, Tabuchi M, Ujihara T, Takeda Y and Ikuta H 2011 *Appl. Phys. Express* **4** 083102
[23] Huang Q, Zhao J, Lynn J W, Chen G F, Luo J L, Wang N L and Dai P 2008 *Phys. Rev. B* **78** 054529
[24] Zhao J, Huang Q, de la Cruz C, Li S, Lynn J W, Chen Y, Green M A, Chen G F, Li G, Li Z, Luo J L, Wang N L and Dai P 2008 *Nat. Mater.* **7** 953
[25] Díaz A, Mechin L, Berghuis P and Evetts J E 1998 *Phys. Rev. B* **58** R2960
[26] Verebelyi D T, Christen D K, Feenstra R, Cantoni C, Goyal A, Lee D F, Paranthaman M, Arendt P N, DePaula R F, Groves J R and Prouteau C 2000 *Appl. Phys. Lett.* **76** 1755
[27] Chiara T, Iida K, Hänisch J, Kurth F, Jaroszynski J, Sumiya N, Chihara M, Hatano T, Ikuta H, Schmidt S, Seidel P, Holzapfel B and Larbalestier D C 2016 *Sci. Rep.* **6** 36047
[28] Matsumoto T, Kondo K, Hatano T, Iida K and Ikuta H in preparation
[29] Straumal B B, Bokshtein B S, Straumal A B and Petelin A L 2008 *JETP Letters* **88** 537
[30] Wang C, Li Y K, Zhu Z W, Jiang S, Lin X, Luo Y K, Chi S, Li L J, Ren Z, He M, Chen H, Wang Y T, Tao Q, Cao G H and Xu Z A 2009 *Phys. Rev. B* **79** 054521
[31] Kim S K, Tillman M E, Kim H, Kracher A, Bud'ko S L, Prozorov R and Canfield P C, 2010 *Supercond. Sci. Technol.* **23** 054008

Supplementary information

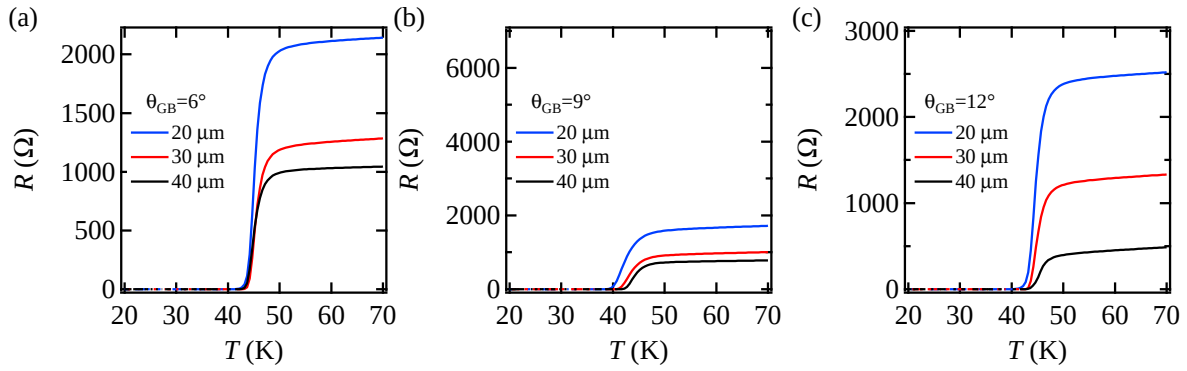

Figure S1. (Color online) Temperature dependence of the resistance curves for the inter-grain bridges, (a) θ_{GB}=6°, (b) θ_{GB}=9° and (c) θ_{GB}=12°, having various bridge width.

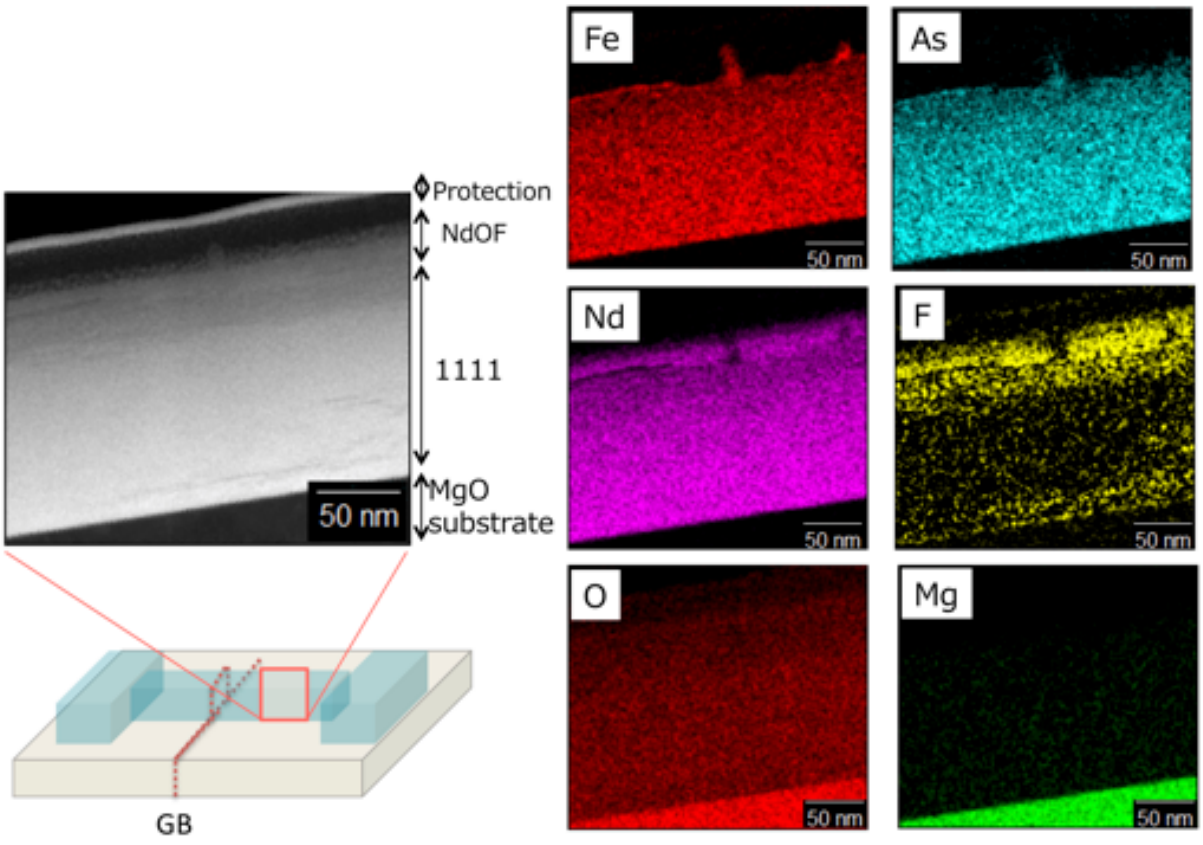

Figure S2. (Color online) Cross-sectional TEM micrograph and elemental mappings acquired at a position away from the GB region. The micro-bridge used for this observation is the one with (θ_{GB}=24°) reported in our previous study [19]. Note that the NdOF over-layer was not removed.

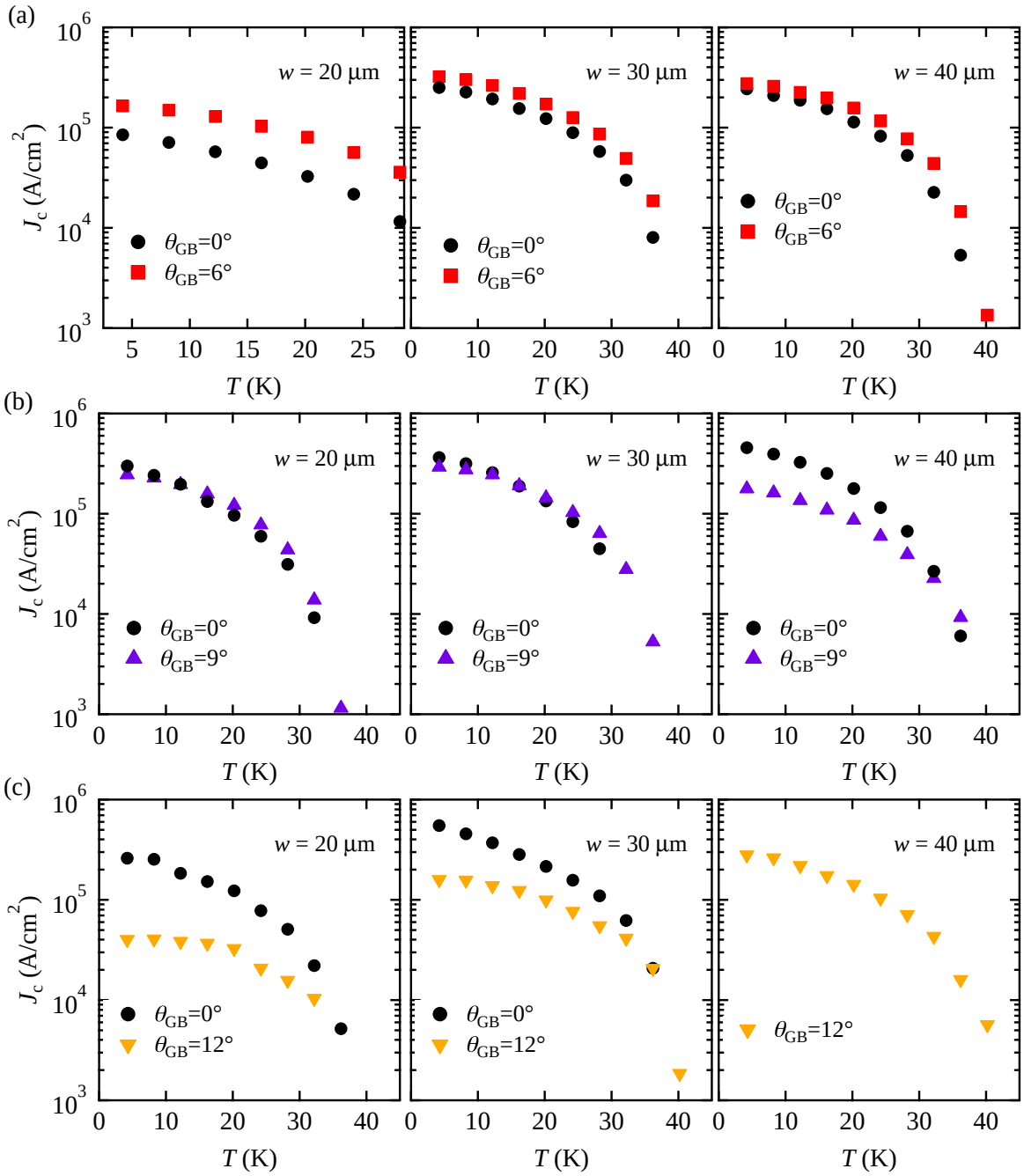

Figure S3. (Color online) Temperature dependence of the self-field Jc for the intra- (θ_{GB}=0°) and inter-grain bridges, (a) θ_{GB}=6°, (b) θ_{GB}=9° and (c) θ_{GB}=12°, having various bridge width, w. For θ_{GB}=12° the 40 μm-wide bridge for intra-grain measurements was damaged and, therefore, the data was not available.